Research Article

Journal of Environmental Nanotechnology

Fabrication and Characterization of High-performance Nanocellulose-reinforced Apple Leather Composites for Sustainable Applications

S. Sheeju Selva Roji[1], Rakesh Adakane[2], A. Elaiyaraja[3*], S. Duraithilagar[4] and P. Praveenkumar[5]

[1]Department of Mechanical Engineering, University College of Engineering Nagercoil, Kanyakumari, TN, India
[2]Department of Mechanical Engineering, Yeshwantrao Chavan College of Engineering, Nagpur, MH, India
[3]Department of Master of Business Administration, Panimalar Engineering College, Chennai, TN, India
[4]Department of Mechanical Engineering, Vinayaka Mission's Kirupananda Variyar Engineering College, Vinayaka Mission's Research Foundation (Deemed to be University), Salem, TN, India
[5]Industrial Safety and Engineering, Vinayaka Mission's Kirupananda Variyar Engineering College, Vinayaka Mission's Research Foundation (Deemed to be University), Salem, TN, India
Received: 25.03.2026 Accepted: 30.05.2026 Published: 30.06.2026
*illayar018@gmail.com

ABSTRACT

The accumulation of apple leather scrap waste from footwear industries creates serious environmental disposal problems and limits the sustainable utilization of leather by-products. In the present study, an eco-friendly nanocomposite material was developed by reinforcing apple leather scrap fibers with cellulose nanocrystals (CNC) extracted from timoho (Kleinhovia hospita) plant fibers, along with green synthesized nanoparticles such as ZrO_2, SiO_2, and ZnO and isoprene rubber latex as a binder. Nanocellulose was produced through alkali treatment, bleaching, and sulfuric acid hydrolysis, followed by ultrasonication to obtain nanoscale cellulose particles. The composite sheets were fabricated through mechanical mixing, molding, hydraulic pressing (1500–2000 psi), and thermal curing at 70 °C, and their structural, thermal, and mechanical properties were evaluated using FT-IR, XRD, FESEM, DLS, TGA, and mechanical testing. The results showed that the synthesized nanocellulose exhibited a crystallinity index of about 82% and particle size of 272 nm, confirming successful formation of crystalline nanofibers. Mechanical analysis revealed significant improvements in composite performance after CNC incorporation, where the tensile strength increased from 1.55 to 1.82 N mm^{-2} in the control composite and reached a maximum of 3.33 N mm^{-2} in the ZrO_2–CNC reinforced composite. Similarly, the simple tear strength increased from 14.29 to 16.67 N mm^{-1}, while the stitch tear strength improved from 14.29 to 16.80 N mm^{-1} for the CNC-reinforced composites. Thermal analysis also demonstrated improved stability, with major degradation occurring around 335–345 °C. These results confirm that nanocellulose-reinforced apple leather composites exhibit enhanced mechanical strength and thermal stability. The developed materials show promising potential for sustainable footwear components, eco-friendly leather substitutes, packaging materials, and flexible composite products, contributing to waste valorization and environmentally responsible material development.

Keywords: Nanocellulose; Green synthesis; Mechanical behaviour; Thermal stability; Tear strength.

1. INTRODUCTION

The development of efficient strategies for converting waste materials into value-added products has become a significant focus within the scientific community in recent years. Such approaches can effectively reduce industrial waste generation while simultaneously mitigating environmental pollution. Sustainable national development strongly relies on environmentally responsible industrial production processes that minimize adverse impacts on terrestrial ecosystems. Apple leather enriched with encapsulated pomegranate seed oil was developed with chitosan–soy protein isolate complex particles to stabilize oil emulsions. The 20% oil emulsion exhibited the lowest creaming index and droplet size of about 1 µm with Newtonian flow behavior. Sensory evaluation indicated that the addition of up to 0.2% pomegranate seed oil emulsion maintained acceptable color and overall acceptability similar to the control sample (Javadi *et al.* 2023). Infrared spectroscopy showed strong correlations with moisture content, sugar composition and acidity, demonstrating its effectiveness as a rapid and non-destructive technique for determining physicochemical properties in apple fruit leather production (Nizamlioglu *et al.* 2022). Apple fruit leather enriched by acáchul (Ardisia compressa) powder, stevia, and maltitol syrup was developed and evaluated for bioactive compounds, texture, and sensory characteristics. The product exhibited notable antioxidant capacity, high polyphenol and anthocyanin contents, and approximately 91% antioxidant bio accessibility (Vázquez-Sánchez *et al.* 2021).

Nanocellulose was extracted from corn cob agricultural waste using ultrasonic-assisted sulfuric acid hydrolysis. The process produced nanocrystalline cellulose with crystallinity ranging from 63.55–71.76% and nanoparticle sizes between 15.3 and 2.1 nm. Characterization through SEM, TEM, XRD, and FTIR confirmed removal of hemicellulose and lignin and demonstrated an eco-friendly, cost-effective method for producing nanocellulose with high yield. Micro/nanocellulose fibers were extracted from Lygeum spartum, a Mediterranean plant, using combined alkali and mechanical treatments followed by ultrasonic processing. Thermal and morphological analyses confirmed improved fiber stability and porous structures, highlighting Lygeum spartum as a promising alternative source for nanocellulose production (Ahmima *et al.* 2024).

Bamboo nanocellulose reinforced epoxy composites exhibited improved tensile strength up to 83.92 MPa at 1.5 wt.% loading, demonstrating the importance of optimal filler concentration (Verma *et al.* 2024). Characterization confirmed nanoscale structures with crystallinity around 78.5%, while thermal analysis showed reduced stability for CNC compared with CNF. A recent study demonstrated the potential of PALF as a sustainable source for nanocellulose suitable for applications in biocomposites and biomedical materials (Da Costa *et al.* 2025). PEG-plasticized nanocellulose membranes incorporated with ZnO nanoparticles (1–5%) were developed for biomedical applications. Structural and biological analyses revealed improved mechanical strength, antibacterial activity, and cytocompatibility with increasing ZnO content (Unni *et al.* 2025).

Synthetic isoprene rubber latex was utilized for 3D printing of elastomers via vat photopolymerization. Thermal post-processing produced elastomers with elongation at break ranging from 94–682%, demonstrating their suitability for complex elastomeric structures (Wen *et al.* 2024). Methacrylate-functional liquid isoprene rubber was employed for additive manufacturing using digital light processing. Photo-induced thiol-click reactions enabled efficient crosslinking, while divinyl ethers reduced viscosity and accelerated curing. The optimized formulation produced precise elastomeric structures with feature sizes of approximately 0.5 mm (Strohmeier *et al.* 2020). A chemical assembly rubber was developed by grafting 4-aminopyridine onto epoxidized isoprene rubber and Eucommia ulmoides gum to form a dynamic hydrogen-bonding network. The hydrogen bonding enhanced strain-induced crystallization and improved nano-filler dispersion within the rubber matrix. The resulting material exhibited higher modulus, tensile strength, and tear resistance, along with reduced heat build-up during dynamic loading (Wang *et al.* 2026). Thermoplastic elastomers were prepared using polyvinyl chloride, polyethylene terephthalate, and butyl rubber to study their compatibility and performance. The incorporation of plastics influenced curing behavior, thermal stability, and solvent resistance of the elastomers (Madani and Movahed, 2024). Microscopic deformation behavior of crosslinked isoprene rubber was examined by atomic force microscopy. The study revealed heterogeneous deformation at nanoscale rather than classical affine deformation behavior. Additionally, strain-induced crystallization structures (~10 nm) were directly observed, providing insight into the self-reinforcing mechanisms of crystalline rubber (Liang *et al.* 2025).

Effect of curing agents at vulcanization behavior of silica-filled isoprene rubber composites was investigated by Zn@SiO_2 as a dual-function filler. The modified composites exhibited increased stiffness but reduced fracture toughness, demonstrating the influence of curing agent distribution on mechanical properties (Mostoni *et al.* 2022). Pd nanocatalysts supported on substoichiometric oxides (TiO_2, ZnO, ZrO_2) were prepared using a green laser synthesis method. The catalysts exhibited excellent catalytic performance in carbon–carbon bond forming reactions, achieving 100% conversion of bromobenzene to biphenyl under mild conditions (Das *et al.* 2020). Plant extracts from Zingiber officinale and Syzygium aromaticum were used to synthesize ZnO: ZrO_2 nanocomposites through a green method. Characterization confirmed polycrystalline nanoparticles with average sizes of 33–37 nm (Tuama and Alias, 2024). A ZnO/ZrO_2 nanocomposite was synthesized using a green combustion method with Butea monosperma leaf powder as fuel. Structural analyses confirmed hexagonal ZnO and cubic ZrO_2 phases with spherical nanoparticles (Sathisha *et al.* 2025). A green synthesized ZrO_2/CuO–ZnO nanocomposite was prepared using Corallocarpus epigaeus rhizome extract. Structural and spectroscopic analyses confirmed successful nanoparticle formation with improved optical properties. The nanocomposite exhibited enhanced antibacterial, antifungal, and α-amylase inhibition activities compared to pure ZrO_2 nanoparticles (Shailaja *et al.* 2023). The composite containing 75% leather fiber and 25% jute fiber exhibited superior performance with a tensile strength of 3.57 MPa, lower water absorption, and enhanced thermal stability up to 353°C (Dhar *et al.* 2026). SEM, FTIR, and XRD analyses confirmed the structural modifications and improved interfacial bonding after chemical treatment of the fibers. Similarly, chemically treated neem twig fibers exhibited enhanced tensile strength (8.97 MPa) and improved thermal stability, indicating their potential as sustainable reinforcement materials for biodegradable composites (Raja and Devarajan, 2024).

Sustainable poly(lactic acid) (PLA) composites reinforced with nanocellulose from waste cellulose fibers were developed and they showed significant improvements in elongation, impact strength, and toughness compared to neat PLA (Mahmud *et al.* 2020).

Timoho fiber was treated with different NaOH concentrations to improve their properties for green composite reinforcement. Alkali treatment improved crystallinity, cellulose content, density, and tensile strength of the fibers. The FTIR and SEM analyses confirmed the removal of hemicellulose and impurities, resulting in improved surface roughness and better matrix adhesion (Gapsari *et al.* 2021).

To the best of our knowledge, no previous studies have reported extraction of cellulose nanocrystals (CNC) from the timoho tree. The novelty of the work lies in the extraction and characterization of CNC from timoho fibers and subsequent fabrication of synthetic composite sheets from apple leather waste reinforced with CNC using isoprene rubber and other suitable binders. Since finished apple leather products constitute a significant portion of solid apple leather waste, transforming this waste into value-added consumer products represents an economically viable approach for reducing environmental pollution while simultaneously generating additional revenue. Therefore, the objective of this experimental investigation is to develop apple leather composite sheets using apple leather scraps reinforced with CNC derived from plant fibers and bonded with isoprene rubber latex. The prepared composites were evaluated in terms of their physical, thermal, and mechanical properties. Furthermore, present study focuses on extraction and modification of natural nanofibers from timoho and their comprehensive characterization using various standard analytical techniques. The potential application of the synthesized nanofibers as reinforcement materials in biocomposites derived from apple leather scrap waste was also explored.

2. MATERIALS AND METHODOLOGY

2.1 Materials

Apple leather scraps were collected from local footwear manufacturing units in Ambur, Tamil Nadu, which is well known for leather processing industries. Natural plant fibers were collected from agricultural fields in Pollachi, Coimbatore district, Tamil Nadu, and used as the raw material source for nanocellulose extraction. Various chemicals used in this study are zinc oxide, zirconium dioxide, silica, natural rubber latex, isopropyl alcohol, ethylene glycol, polyurethane binder, filler wax, casein binder, NC lacquer, pigment, sodium chlorite, sodium hydroxide and sulfuric acid. All chemicals were of analytical grade and were procured from Merck India and authorized chemical suppliers in Coimbatore, Tamil Nadu.

2.2 Methodology

2.2.1 Nanocellulose Extraction from Timoho Fiber

Nanocellulose crystals (NCC) were prepared from timoho fibers (Kleinhovia hospita) through sequential chemical purification followed by controlled acid hydrolysis. Initially, the extracted timoho fibers were thoroughly washed with distilled water to eliminate impurities and dust and then dried in a hot air oven at 60 °C for 24 hours. The dried fibers were subjected to alkali treatment using 5 wt.% NaOH solution at 80 °C for 2 hours to eliminate hemicellulose, waxes, and other non-cellulosic substances (Gapsari *et al.* 2022a). After the alkali treatment, the fibers were repeatedly washed with distilled water until neutral pH was obtained. The purified fibers were further bleached using 2 wt.% sodium chlorite in acidic medium at 70 °C for about 1 hour to eliminate lignin and to obtain purified cellulose fibers.

The resulting cellulose was then subjected to acid hydrolysis using 60–65 wt.% sulfuric acid at 45 °C for 45 min with continuous stirring. During this step, amorphous regions of cellulose were selectively hydrolyzed, leaving behind highly ordered crystalline domains (Abdel-Hamied *et al.* 2022). The hydrolysis reaction was terminated adding excess cold distilled water, followed by centrifugation to eliminate excess acid and repeated washing. The suspension was then dialyzed with DI water until neutral pH was achieved to ensure complete elimination of residual acid. Finally, the suspension was ultrasonicated for 20–30 min, which separated the crystalline domains and reduced particle aggregation, resulting in nanocellulose crystals typically having diameters of about 5–20 nm and lengths of 100–300 nm. The obtained nanocellulose suspension was subsequently dried for further use as a reinforcement material.

2.2.2 Green synthesis of ZrO_2–SiO_2–ZnO Nanoparticles

The green synthesis of ZrO_2, SiO_2, and ZnO nanoparticles was carried out using environmentally benign routes. For ZrO_2 nanoparticles, zirconyl nitrate hydrate (ZrO $(NO_3)_2 \cdot xH_2O$) was used as the precursor, while Moringa oleifera leaf extract acted as reducing and stabilizing agent. Fresh leaves were washed, boiled in DI water at 70 °C for 25 min, and filtered to obtain the extract. A 0.1 M zirconyl nitrate solution was prepared in distilled water, and the plant extract was added dropwise under continuous magnetic stirring at 70 °C for 2 hours. The precipitate was centrifuged, washed with distilled water and ethanol, dried at 100 °C for 12 hours, and calcined at 500 °C for 3 hours to obtain crystalline ZrO_2

nanoparticles (Febriantini *et al.* 2025). For SiO_2 nanoparticles, rice husk ash was used as a sustainable silica source. The ash was treated with 2 M NaOH at 90 °C for 2 hours to produce sodium silicate solution, which was filtered and subsequently titrated with 1 M HCl until pH 7 to form silica gel. The gel was aged for 12 hours, washed with DI water, and dried at 100 °C to obtain amorphous SiO_2 nanoparticles (Nabil *et al.* 2023). In the case of ZnO nanoparticles, zinc acetate dihydrate served as the precursor, while Aloe vera leaf extract was used as the green reducing agent. The plant extract was prepared by boiling 10 g of Aloe vera gel in 100 mL DI water at 70 °C for 20 min and filtering the solution. A 0.1 M zinc acetate solution was mixed with the extract and stirred at 70 °C for 1 hour, followed by adjustment of pH to 10–11 using NaOH to get $Zn(OH)_2$. The precipitate was washed, dried at 90 °C for 12 hours and calcined at 400 °C for 3 hours to obtain ZnO nanoparticles (Ahamed *et al.* 2023). The synthesized nanoparticles typically exhibit particle sizes in the 10–50 nm range.

2.2.3 Extraction of Apple Leather Fiber

The apple leather was prepared using fresh apples as the primary raw material. Approximately 220 g of apples was first washed thoroughly, cored, and cut into small pieces. The apple pieces were then blended to obtain a smooth puree. After blending, the required amount of prebiotics (agavins or inulin) was added to the puree in the form of an aqueous solution containing 50 mL of 1% citric acid, according to the experimental formulation. The resulting mixture was subjected to heat treatment at 75 ℃ for 10 minutes to improve stability and ensure uniform mixing. The heated puree was then spread evenly onto trays lined with cellophane paper to form thin layers. Subsequently, the trays were placed in a tray dryer and dried at 60 ℃ for about 5 hours with an air velocity of 2 m/s until a flexible leather-like sheet was obtained. After drying, a portion of the apple leather was analyzed immediately (García-García *et al.* 2019).

2.2.4 Preparation of Reference Samples

Table 1. Composition of the control sample

Sample Number	Apple Leather Waste (%)	Rubber Content (%)	Ethylene Glycol (mL)
1	25	75	-
2	35	65	0.5
3	45	55	0.5
4	55	45	0.5
5	65	35	0.5

The reference samples were prepared to compare the performance of the modified composite samples. The samples were fabricated under controlled conditions to maintain consistency and ensure accurate evaluation of the experimental results. Apple leather scraps were blended with isoprene rubber in different proportions to optimize the composite properties, as presented in Table 1.

During the composite synthesis process, apple leather fibers obtained from scrap materials were incorporated at weight fractions of 25%, 35%, 45%, 55%, and 60%. These fibers were blended with natural isoprene rubber at corresponding proportions of 75%, 65%, 55%, 45%, and 35%, respectively, while the amount of ethylene glycol was kept constant in each formulation. The isoprene rubber served as the binding agent, whereas ethylene glycol functioned as the plasticizer. Based on the evaluation of all control experiments, the optimal composite formulation was identified as 45% apple leather scrap fiber combined with 55% isoprene rubber in the presence of ethylene glycol.

2.2.5 Stabilizer Application Process

Plasticizers are widely incorporated into polymer systems to enhance their flexibility, tensile strength, stitch tear strength, thermal stability and percentage elongation. They also improve the processing characteristics and reduce brittleness of polymeric materials. In the present research, various stabilizer compounds were employed during preparation of the biocomposite materials, as summarized in Table 2.

Table 2. Composition of optimal stabilizer-based composites

Sample Number	Apple Leather Waste (%)	% of Isoprene Rubber	Rubber Content (%)	Stabilizer
01	45%	55%	0.5 mL	Trial 1:2% SiO_2 Trial 2: 2% ZrO_2 Trial 3: 2% ZnO

2.2.6 Preparation of Apple Leather Fiber Composite Sheet

Apple leather scrap composites were prepared through a sequence of steps including waste collection, fiber pretreatment, binder selection, and material compounding to obtain uniform composite sheet. Initially, 7 g of apple fibers from scraps was soaked in DI water for 12 hours and manually chopped. Natural latex was used as a binder to improve adhesion and flexibility within the composite structure. Subsequently, 0.5 mL of ethylene glycol, 14 mL of isoprene rubber, and 2 wt.% each of SiO_2, ZrO_2, and ZnO nanoparticles were gradually incorporated into the chopped fibers. The mixture was then homogenized using a mechanical mixer to produce a uniform composite mixture.

2.3 Shaping and Thermal Curing Process

The final stage of composite fabrication involved shaping and curing of the prepared slurry. The slurry was first poured into a die mold and manually pressed to remove excess water. The moist sheets were then compressed by a hydraulic press (1500 psi for 10 s). The pressed sheets were dried under sunlight for two to three days, followed by a final hot pressing step at 2000 psi and 70 °C for approximately 10 s to produce a dense and durable composite sheet.

2.4 Preparation of Nanocellulose-based Composite

The synthesis of nanocellulose-based scrap apple leather composites involves additional processing steps compared with traditional scrap apple leather composites. Nanocellulose is introduced into the composite mixture as a reinforcing phase to improve the mechanical properties of the material.

Nanocellulose was extracted from timoho plant fibers using a chemical treatment method and dispersed in distilled water through ultrasonication. Apple leather scraps were crushed into smaller particles by a crushing machine. Subsequently, 0.5 mL of ethylene glycol, 14 mL of isoprene rubber, 2 wt.% ZrO_2, apple leather fibers, and nanocellulose were blended to obtain a uniform mixture. The nanocellulose content was varied at 1–3 wt.% relative to apple leather fibers and uniformly dispersed using ultrasonication (Da'na *et al.* 2023). The mixture of apple leather fibers, binder, and nanocellulose was compounded under high pressure to obtain the composite material. The scrap apple leather composite was molded into the desired shape. A protective coating was applied to composite surface to enhance durability and prevent stains, scratches, and other surface damage.

2.5 Characterization of Nanocellulose and Composite

The synthesized nanofibers and apple leather composite sheets were characterized using various analytical techniques to determine their thermal, physicomechanical, chemical, and morphological properties. Physicomechanical evaluations included stitch tear strength, tensile strength, flexing index, elongation at break and water absorption tests to assess the performance of the materials.

2.5.1 FT-IR and TGA Analysis

FT-IR spectroscopy (SHIMADZU) was used to analyze cellulose nanofibers and apple leather composite sheets to identify the characteristic functional groups present in the fiber structure (Yu *et al.* 2022). The thermal stability of nanocellulose and the synthesized nanocomposites was assessed using thermogravimetric analysis (TGA) conducted on a thermo-analyzer.

2.5.2 XRD Analysis

X-ray diffraction (XRD) analysis was conducted to evaluate crystalline characteristics of nanocellulose fibers and corresponding composite sheets. The measurements were carried out using a Bruker Advance D8 instrument. The diffraction patterns obtained from the analysis were recorded as intensity counts against diffraction angles (2θ), and the corresponding peak positions are summarized in the table as well as represented in the form of x–y diffraction plots. Based on the diffraction data, the crystallinity index of the samples was estimated using the following equation, which provides a convenient approach to quantify the degree of crystalline ordering within the material structure (Unni *et al.* 2022):

$$\mathrm{CI} = \frac{I_{max} - I_{min}}{I_{max}} \times 100\% \quad \ldots (1)$$

2.5.3 FESEM Analysis

Field emission scanning electron microscopy (FESEM) was employed to investigate the surface topography of the fibers. The analysis was conducted using a Zeiss, Gemini FESEM instrument at an accelerating voltage of 5 kV, with magnifications varying between 10× and 300,000× to obtain high-resolution images of the fiber morphology.

2.5.4 Dynamic Light Scattering Particle Size Analysis

The particle size distribution of cellulose nanocrystals in suspension was measured using a dynamic light scattering analyzer (Litesizer 500, Anton Paar, Austria).

2.6 Mechanical Behavior of Composite Material

2.6.1 Tensile Strength

The tensile strength of a material is a crucial mechanical parameter used to evaluate its structural performance under applied stress. It represents maximum stress specimen can withstand before fracture happens. In this study, the tensile properties of the composite samples were determined. Tensile strength is calculated as the maximum applied force at the point of failure divided by the original cross-sectional area of the specimen (S.-Y. Wang *et al.* 2025)

$$\text{Tensile strength} = \frac{\text{Breaking Load } (N)}{\text{Thickness} \times \text{Width } (\text{mm}^2)} \quad \ldots (2)$$

The tensile properties of the specimens were evaluated. The measurements were performed using a Instron Universal Testing Machine to determine the strength of the samples under applied tensile loading.

2.6.2 Elongation at Break (%)

Elongation refers to increase at length of sample at the moment of fracture, expressed as percentage of its gauge length. This parameter was determined according to the procedures. The percentage elongation of the fiber-reinforced composite was measured in the same Universal Testing Machine. The corresponding percentage elongation values were calculated using equation (3):

$$\% \text{ of Elongation} = \frac{\text{Final length} - \text{Initial length}}{\text{Initial length}} \quad \ldots (3)$$

2.6.3 Stitch Tear Strength

A wire loop of suitable dimensions was inserted through two prepared holes in the specimen before the loading process was initiated (Shakil *et al.* 2025). After fixing the specimen in the designated clamp of the tensile testing equipment, the load required to pull wire through the material was recorded. The experiment was performed in accordance with DIN 53331 standard procedure.

2.6.4 Simple Tear Strength

Tear test specimen was prepared in rectangular shape containing a wide central slit with tapered edges. During testing, the tensile machine applied a pulling force that caused the slit to open, leading to tearing from the tapered ends. The maximum load required to continue the tear and the thickness of the specimen were recorded.

2.6.5 Water Absorption

For water absorption analysis, specimens were initially placed in an oven at 115 °C for 10 min to eliminate residual moisture. After drying, the samples were transferred to a desiccator and allowed to cool to room temperature. Once cooled, the specimens were weighed to obtain their initial mass. The samples were then immersed in water maintained at 23 °C for 24 hours to allow moisture uptake until equilibrium was reached. Following immersion, the specimens were taken out of water, gently wiped with lint-free cloth to eliminate surface moisture, and weighed again.

$$\text{Percentage (\%) of water absorption of the sample} = \frac{w_2 - w_1}{w_1} \times 100\% \quad \ldots (4)$$

Here, W1 denotes the mass of the specimen prior to water immersion, whereas W2 indicates the mass of the specimen after the water absorption process.

2.6.6 Moisture Absorption

Moisture content is an important parameter for evaluating and maintaining the quality of materials in various industrial applications. In this study, the moisture level of composite samples was determined by thermal drying method. The specimens were heated to remove the absorbed moisture, and the reduction in sample weight was recorded periodically until a constant mass was achieved.

3. RESULTS AND DISCUSSION

The characterization of timoho fibers using various standardized analytical methods provided insights into structural morphology and physicochemical properties of cellulose nanofibers.

3.1 FT-IR Spectra of Fiber Samples

The FT-IR spectrum of untreated timoho fibers exhibited prominent peaks at 3262 cm^{-1} and 2877 cm^{-1}, corresponding to O–H stretching and C–H vibrations, respectively (Fig. 1). These functional groups originate from cellulose, hemicellulose, and lignin components naturally present in the fibers. A distinct peak observed near 1661 cm^{-1} was due to the carbonyl (C=O) groups present in hemicellulose and lignin structures. This peak disappeared in the spectra of chemically bleached cellulose fibers, indicating the removal or modification of these constituents. The bleaching treatment with peracetic acid likely promoted oxidation of C–OH groups to carbonyl groups, resulting in a sharper and stronger peak in the oxidized cellulose samples. All fiber samples displayed a peak around 1510 cm^{-1}, attributed to aromatic ring vibrations, confirming the presence of organic compounds. In contrast, the absence of a peak at 1102 cm^{-1} in CNC suggests structural changes in surface functional groups. A peak near 852 cm^{-1} corresponds to C–O within cellulose.

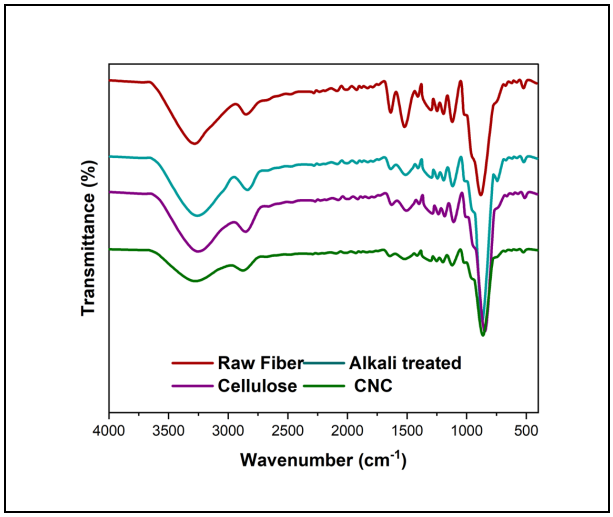


Fig. 1: FT-IR analysis of fiber samples

3.2 XRD Characterization of Nanocellulose

X-ray diffraction (XRD) analysis was performed to investigate the crystalline structure of oxidized cellulose nanocrystals (Fig. 2). The diffraction

pattern displayed distinct peaks associated with specific lattice planes. A major peak appeared at 2θ = 24.57° and a minor peak near 38.67° suggest the presence of cellulose-related crystalline phases.

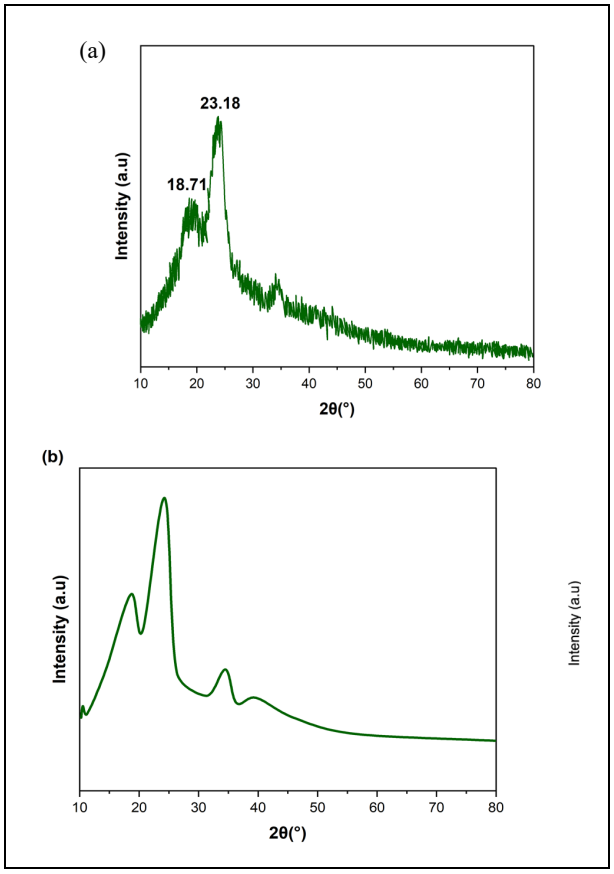


Fig. 2: (a) XRD pattern of oxidized nanocellulose and (b) crystallinity by segal equation

The crystallinity index of oxidized CNC was determined using the Segal method, yielding a value of 82%, indicating a high crystalline content. Such enhanced crystallinity suggests potential suitability for applications in nanocomposite fabrication, biomedical materials, and packaging technologies, providing important information about the structural properties of the material.

3.3 TGA of Timoho Fibers

The thermal stability of the fiber samples was evaluated using TGA 8000 (PerkinElmer, USA). Approximately 6–10 mg of each sample was heated in a platinum crucible under nitrogen from room temperature to 700 °C at 10 °C min^{-1}. The recorded TGA/DTG curves (Fig. 3) indicate two distinct thermal degradation stages for the fibers.

In the initial stage of TGA (50–120 °C), only about 4% weight loss was observed, mainly due to the evaporation of moisture from the fibers. Alkali treatment reduced weight loss by removing lignin and other amorphous components from fiber surface. The DTGA and TGA curves of raw and treated fibers showed similar degradation trends. The maximum weight loss (~72%) occurred around 380 °C due to the decomposition of lignin and char components, indicating fragmentation and degradation of cellulose chains within the fiber structure.

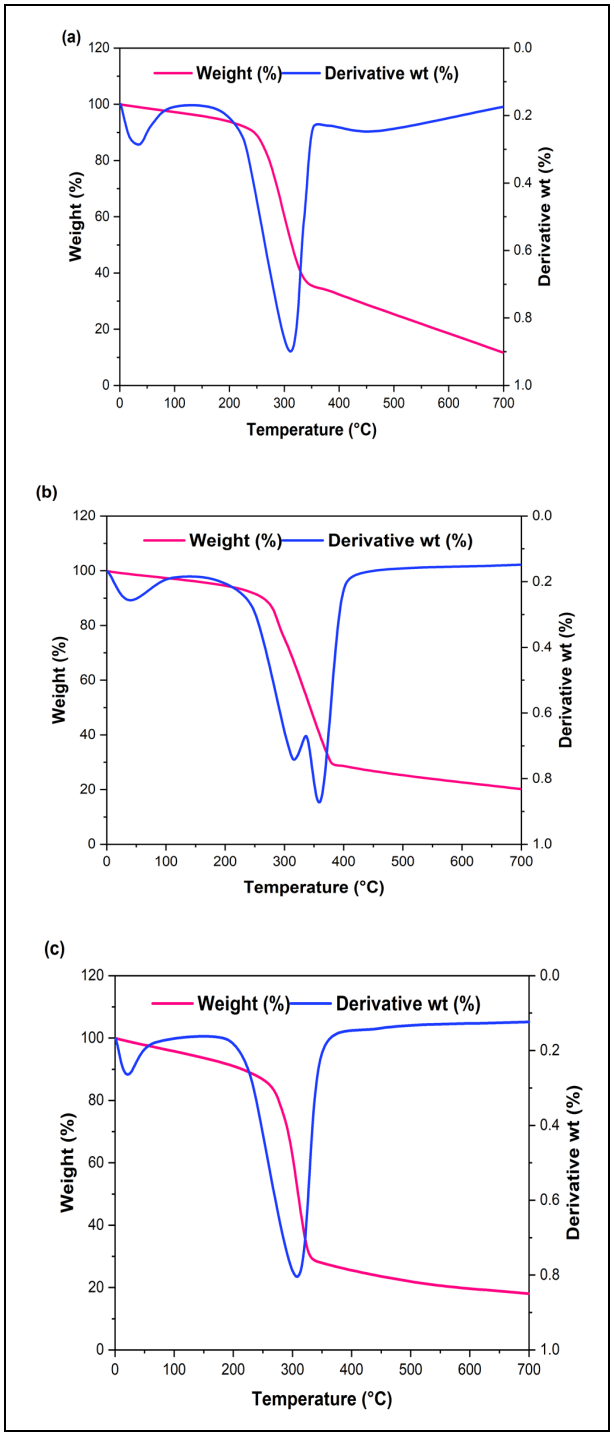


Fig. 3: (a) TGA–DTGA of raw fiber, (b) TGA–DTGA of alkali fiber and (c) TGA–DTGA of treated fiber

3.4 FESEM Analysis of Timoho Fibers

The surface morphology of untreated and alkali-modified timoho fibers was examined using FESEM at various magnifications (Fig. 4). Raw fibers displayed impurities and matrix components such as lignin, hemicellulose, and pectin. These surface materials were noticeably reduced after 5% NaOH treatment and almost completely removed following 10% NaOH treatment.

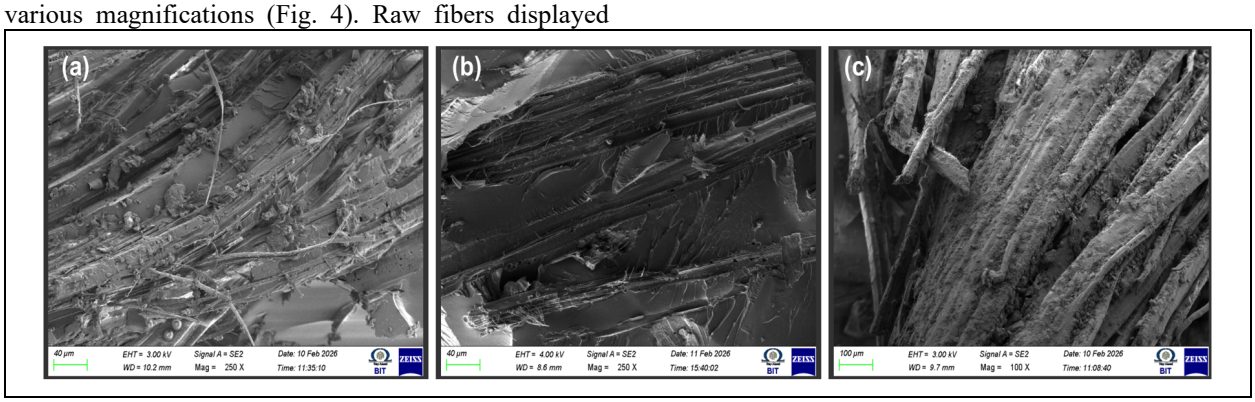


Fig. 4: (a) Raw fiber FESEM Image, (b) FESEM of 5% NaOH fiber and (c) FESEM of 10% NaOH fiber

3.5 Dynamic Light Scattering of Timoho Fibers

3.5.1 Particle Size of Oxidized Nanocellulose

The particle size distribution of crystalline nanocellulose (CNC) obtained through acid hydrolysis and oxidation methods was determined by DLS analysis. The nanocellulose synthesized by oxidation process exhibited particle size of 272 nm as illustrated in Fig. 5.

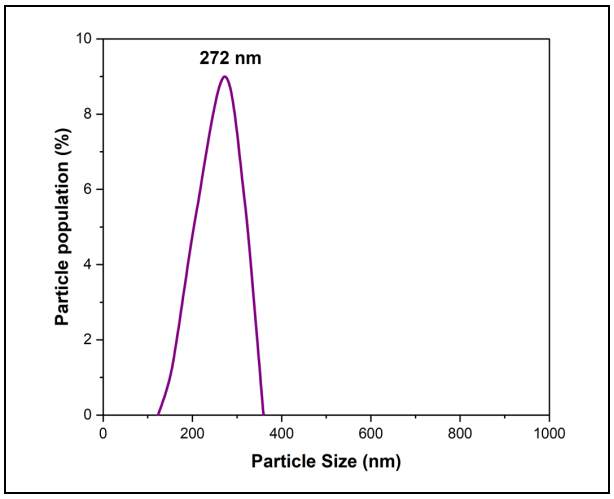


Fig. 5: DLS particle size of CNC

Nanocellulose dimensions influence of the mechanical composite and thermal behavior. Reduced particle size increases surface area, improving dispersion and interfacial bonding with the matrix, thereby enhancing overall composite performance.

3.6 TGA of Control and Composite Samples

Fig. 6 illustrates the thermal degradation of the control and apple leather biocomposites between 50–600 °C. The TGA curves show a two-stage degradation pattern. An initial weight loss of about 3.5% occurs due to moisture and volatile evaporation. A major weight loss of around 65% at approximately 350 °C indicates the decomposition of organic constituents. Overall, about 85% weight reduction was observed at 600 °C, while nearly 15% residual mass remained, representing thermally stable or non-volatile components in the composite.

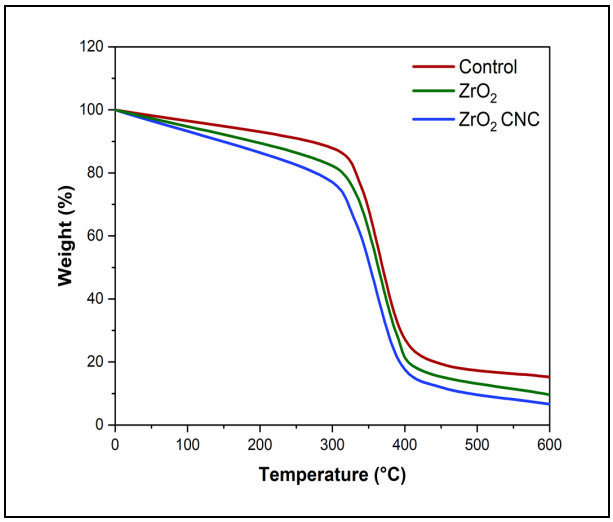


Fig. 6: TGA comparison of nanocellulose composites

Fig. 6 shows an initial weight loss of 4% and 4.5% for the ZrO_2 composite and ZrO_2–nanocellulose composite, respectively, mainly due to moisture removal. The major weight loss (~90%) occurred at 335 °C and 345 °C, indicating significant thermal degradation. Shoulder peaks in the TGA curves suggest the decomposition of natural fibers. The ZrO_2–nanocellulose composite exhibited higher thermal stability than the ZrO_2 composite, likely due to the incorporation of nanocellulose, which improved the thermal resistance of the composite structure.

3.7 XRD Pattern of Nanocellulose Composite

Fig. 7 presents the XRD pattern of the nanocellulose-reinforced composite. The diffraction pattern illustrates the positions and intensities of peaks associated with crystallographic planes of materials within the composite structure. Distinct and sharp peaks indicate an ordered atomic arrangement in the crystalline lattice, reflecting the presence of crystalline phases. In this study, the nanocellulose composite exhibited several diffraction peaks related to cellulose nanofibrils, with a prominent peak appearing at 2θ = 21.82°, corresponding to a characteristic cellulose crystalline plane.

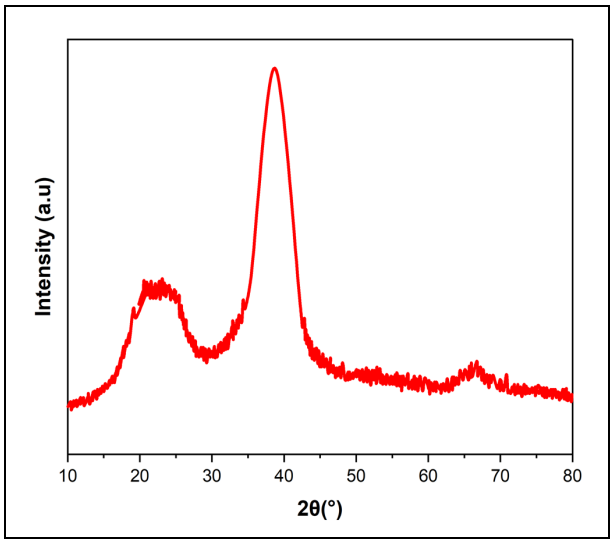


Fig. 7: XRD pattern of CNC composite

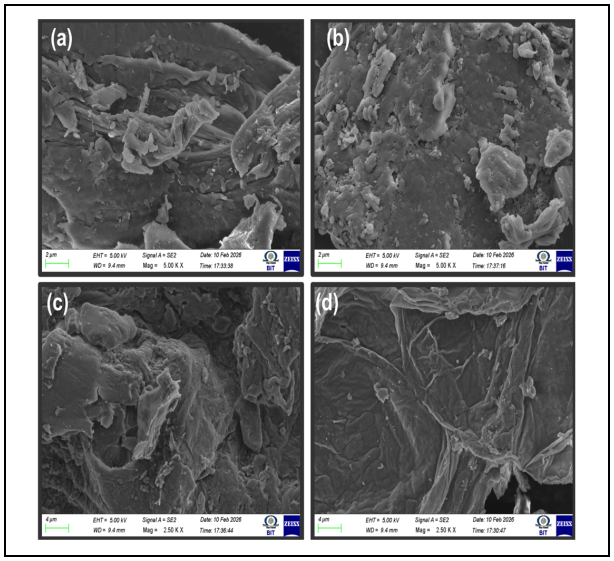


Fig. 8: Cross-sectional FESEM of CNC composite

3.8 FESEM Analysis

Fig. 8 presents the cross-sectional FESEM micrographs illustrating distribution and alignment of cellulose nanofibers. Images clearly show both apple leather fibers and nanofibers embedded in the structure. Interaction between timoho nanofibers and apple leather fibers is evident within the composite framework. Additionally, micrographs provide details about layer thickness, structural uniformity, and interfacial adhesion between nanofibers and the matrix. Such morphological evaluation is essential for improving composite fabrication processes and mechanical performance of the advanced materials.

3.9 Mechanical Characteristics

3.9.1 Tensile Strength

The tensile strength behavior of the composites with and without oxidized cellulose nanocrystals is illustrated in Fig. 9. The control composite without CNC exhibited a tensile strength of approximately 1.55 N mm^{-2}, which increased to about 1.82 N mm^{-2} after the incorporation of oxidized CNC. A similar enhancement was observed for the nanoparticle-reinforced composites. The ZrO_2-based composite showed a tensile strength of about 2.82 N mm^{-2} without CNC, which increased significantly to approximately 3.33 N mm^{-2} with oxidized CNC. Likewise, the SiO_2 composite demonstrated an improvement from 1.96 N mm^{-2} to around 2.24 N mm-2after CNC addition. In the case of the ZnO-reinforced composite, the tensile strength increased from approximately 2.46 N mm^{-2} to about 2.78 N mm^{-2} with oxidized CNC incorporation. Overall, the incorporation of oxidized CNC improved the tensile performance of all composites, indicating enhanced interfacial bonding among reinforcement particles and polymer matrix, which contributed to raised load transfer and mechanical stability of the nanocomposite system.

The elongation behavior of composites with and without cellulose nanocrystals is presented in Fig. 10. The control composite exhibited an elongation value of approximately 22 N without CNC, which increased to about 26 N after the incorporation of CNC. A similar increasing trend was observed for nanoparticle-reinforced composites. The ZrO_2-based composite showed an elongation value of around 66 N, which increased to approximately 73 N with CNC addition. Likewise, the SiO_2 composite demonstrated an improvement from about 35 N to nearly 39 N after CNC incorporation. In the case of the ZnO-reinforced composite, the elongation increased from approximately 48 N without CNC to about 54 N with CNC reinforcement. These results show that incorporation of CNC enhanced elongation behavior of composites, suggesting improved flexibility and better load distribution within the nanocomposite structure. In another study, timoho fiber reinforced polyester composites containing iron powder filler improved impact toughness (126.74 kJ/m^2), and modulus of elasticity. However, elongation decreased with increasing

filler content, while thermal stability of the composites improved (Gapsari *et al.* 2022b).

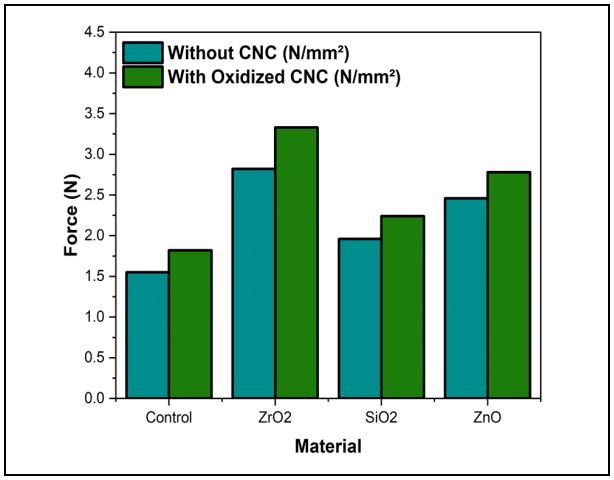


Fig. 9: Tensile strength comparison of composites

3.9.2 Elongation at Break (%)

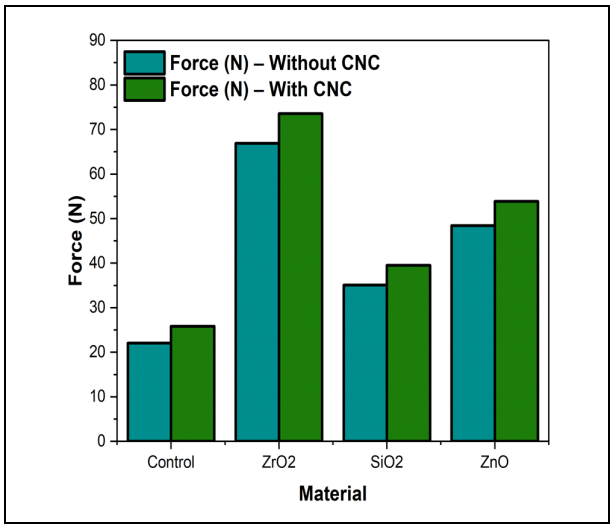


Fig. 10: Elongation comparison of composites

3.9.3 Simple Tear Strength

The simple tear behavior of the composites with and without cellulose nanocrystals is presented in Fig. 11. The control composite exhibited a simple tear strength of approximately 14.29 N/mm without CNC, which increased to about 16.67 N/mm after the incorporation of CNC. A similar improvement was observed for the nanoparticle-reinforced composites. The ZrO_2-based composite showed a tear strength of around 23.36 N/mm without CNC, which increased to approximately 25 N/mm with CNC reinforcement. Likewise, the SiO_2 composite demonstrated an increase in tear strength from about 17.02 N/mm to nearly 19.56 N/mm after CNC incorporation. In the case of the ZnO-reinforced composite, the tear strength improved from approximately 22.61 N/mm without CNC to about 25.50 N/mm with CNC addition. These results showed that incorporation of CNC enhanced tear resistance of the composites, suggesting improved interfacial bonding among reinforcement particles and polymer matrix, which contributed to better resistance against crack initiation and propagation.

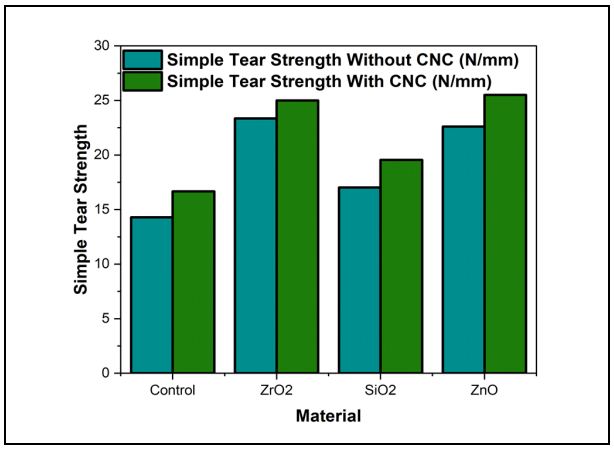


Fig. 11: Tear strength comparison of composites

3.9.4 Stitch Tear Strength

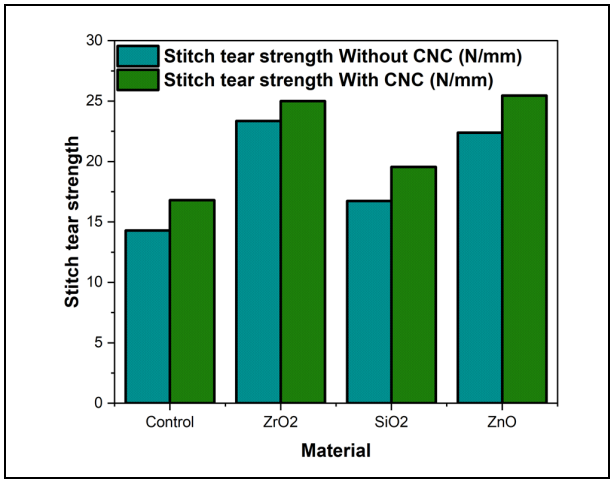


Fig. 12: Stitch tear strength comparison

The stitch tear behavior of the composites with and without cellulose nanocrystals is illustrated in Fig. 12. The control composite exhibited a stitch tear strength of approximately 14.29 N/mm without CNC, which increased to about 16.80 N/mm after the incorporation of CNC. A similar enhancement was observed for the nanoparticle-reinforced composites. The ZrO2-based composite showed a stitch tear strength of around 23.36 N/mm without CNC, which increased to approximately 25 N/mm with CNC addition. Likewise, the SiO_2 composite demonstrated an improvement from about 16.74 N/mm to nearly 19.56 N/mm after CNC incorporation. In the case of the ZnO-reinforced composite, the stitch tear strength increased from approximately 22.39 N/mm without CNC to about 25.45

N/mm with CNC reinforcement. These results indicate that addition of CNC significantly improved stitch tear resistance of the composites, suggesting enhanced interfacial adhesion and improved resistance to crack propagation within the nanocomposite structure.

4. CONCLUSION

Eco-friendly nanocomposite sheets were successfully developed by utilizing apple leather scrap waste reinforced with cellulose nanocrystals extracted from timoho fibers and stabilized with ZrO_2, SiO_2, and ZnO nanoparticles. The chemical treatment and acid hydrolysis process effectively produced crystalline nanocellulose with a crystallinity index of about 82% and particle size of 272 nm, confirming formation of nanoscale cellulose structures suitable for composite reinforcement. Structural analyses using FT-IR, XRD, and FESEM verified the removal of non-cellulosic components and successful incorporation of nanocellulose within the composite matrix. Thermal analysis revealed that the composites exhibited two major degradation stages with significant decomposition occurring around 335–380 °C, indicating good thermal stability. Mechanical evaluation showed that inclusion of CNC significantly enhanced performance of the composites, where tensile strength increased from 1.55 to 1.82 N mm^{-2} in the control composite and reached a maximum of 3.33 N mm^{-2} in the ZrO_2–CNC reinforced composite. Similarly, simple tear strength improved from 14.29 to 16.67 N mm^{-1}, while stitch tear strength increased from 14.29 to 16.80 N mm^{-1} demonstrating improved resistance to crack propagation and better interfacial bonding among reinforcement and matrix. These results confirm that nanocellulose derived from natural plant fibers can effectively enhance thermal and mechanical properties of apple leather waste composites. This approach provides a sustainable pathway for valorizing industrial leather waste into high-value biocomposite materials, which can be potentially applied in footwear components, flexible composite sheets, packaging materials, and other eco-friendly engineering applications.

FUNDING

This research received no specific grant from any funding agency in the public, commercial, or not-for-profit sectors.

CONFLICTS OF INTEREST

The authors declare that there is no conflict of interest.

COPYRIGHT

This article is an open-access article distributed under the terms and conditions of the Creative Commons Attribution (CC BY) license (http://creativecommons.org/licenses/by/4.0/).

REFERENCES

Abdel-Hamied, M., Hassan, R. R. A., Salem, M. Z. M., Ashraf, T., Mohammed, M., Mahmoud, N., El-din, Y. S. and Ismail, S. H., Potential effects of nano-cellulose and nano-silica/polyvinyl alcohol nanocomposites in the strengthening of dyed paper manuscripts with madder: an experimental study, *Sci. Rep.,* 12(1), 19617(2022). https://doi.org/10.1038/s41598-022-23907-1

Ahamed, M., Lateef, R., Khan, M. A. M., Rajanahalli, P. and Akhtar, M. J., Biosynthesis, Characterization, and Augmented Anticancer Activity of ZrO_2 Doped ZnO/rGO Nanocomposite, *J. Func. Biomater*.,14(1) 38(2023). https://doi.org/10.3390/jfb14010038

Ahmima, S., Naar, N., Jędrzejczak, P., Klapiszewska, I., Klapiszewski, Ł. and Jesionowski, T., Isolation and Characterization of Novel Cellulose Micro/Nanofibers from Lygeum spartum Through a Chemo-Mechanical Process, *Polym.*, 16(21), 3001(2024). https://doi.org/10.3390/polym16213001

Da Costa, F. A. T., Dufresne, A., Song, T. and Parra, D. F., Exploring acid hydrolysis conditions and extended mechanical processing for producing cellulose nanocrystal and nanofibrils from pineapple leaf fibers, *Int. J. Bio. Macromol*., 306, 141755(2025). https://doi.org/10.1016/j.ijbiomac.2025.141755

Da'na, E., Hassanin, H. A., Taha, A. and El-Aassar, M. R., Microwave-Aided Green Synthesis of ZrO_2/ZnO/AC Nanocomposite for Catalytic Degradation of Organic Dye, *Water, Air, Soil, Pollut*., 234(7), 436(2023). https://doi.org/10.1007/s11270-023-06451-0

Das, M. K., Bobb, J. A., Ibrahim, A. A., Lin, A., Abouzeid, K. M. and El-Shall, M. S., Green Synthesis of Oxide-Supported Pd Nanocatalysts by Laser Methods for Room-Temperature Carbon-Carbon Cross-Coupling Reactions, *ACS Appl. Mater. Interf*., 12(21), 23844–23852(2020). https://doi.org/10.1021/acsami.0c03331

Dhar, M. C., Shakil, S. R., Hossain, M. A., Shabur, M. A., Nila, U. H. and Mottalib, M. A., Innovative use of tannery solid waste and jute fiber in sustainable leather composites for footwear in Bangladesh, *J. Mater. Cycles Waste Manage.*, 28(2), 1339-1357(2026). https://doi.org/10.1007/s10163-026-02493-8

Febriantini, D., Usman, Rianto, A. K., Pebriani, S., Apriandanu, D. O. B. and Yulizar, Y., Transformation of novel quercetin-facilitated ZrO_2 into ZrO_2@SiO_2–BF_3 nanoparticles: Synthesis, characterization, and catalytic behavior, *Surf. Interf.*, 67, 106589(2025). https://doi.org/10.1016/j.surfin.2025.106589

Gapsari, F., Djakfar, L., Handajani, R. P., Yusran, Y. A., Hidayatullah, S., Rangappa, S. M. and Siengchin, S., The application of timoho fiber coating to improve the composite performance, *Res. Eng.,* 15, 100499(2022a). https://doi.org/10.1016/j.rineng.2022.100499

Gapsari, F., Purnowidodo, A., Hidayatullah, S. and Suteja, S., Characterization of Timoho Fiber as a reinforcement in green composite, *J. Mater. Res. Technol.*, 13, 1305–1315(2021). https://doi.org/10.1016/j.jmrt.2021.05.049

Gapsari, F., Purnowidodo, A., Setyarini, P. H., Suteja, S., Abidin, Z., Rangappa, S. M. and Siengchin, S., Flammability and mechanical properties of Timoho fiber-reinforced polyester composite combined with iron powder filler, *J. Mater. Res. Technol*., 21, 212–219(2022b). https://doi.org/10.1016/j.jmrt.2022.09.025

García-García, A. B., Ochoa-Martínez, L. A., Lara-Ceniceros, T. E., Rutiaga-Quiñones, O. M., Rosas-Flores, W. and González-Herrera, S. M., Changes in the microstructural, textural, thermal and sensory properties of apple leathers containing added agavins and inulin, *Food Chem*., 301, 124590(2019). https://doi.org/10.1016/j.foodchem.2019.03.143

Javadi, F. M., Mirzaee, M. H. and Rajaei, N. A., Study of some qualitative and organoleptic properties of enriched apple leather, *J. Food Sci. Technol*., 19(133), 175–186(2023). https://doi.org/10.22034/FSCT.19.133.186

Liang, X., Nomura, R., Iwabuki, H., Ito, M. and Nakajima, K., Microscopic mechanisms of crosslinked isoprene rubber deformation behavior and strain-induced crystallization study by atomic force microscopy, *Polym.,* 333, 128649(2025). https://doi.org/10.1016/j.polymer.2025.128649

Madani, S. M. and Movahed, S. O., The effect of polyvinyl chloride and polyethylene terephthalate on the mechanical properties of butyl rubber (IIR)-based thermoplastic elastomer using semi-efficient vulcanisation system and a nano zinc oxide as activator, *Plast. Rubb. Compos. Macromol. Eng*., 53(5–7), 143–153(2024). https://doi.org/10.1177/14658011241273527

Mahmud, S., Long, Y., Wang, J., Dai, J., Zhang, R. and Zhu, J., Waste Cellulose Fibers Reinforced Polylactide Toughened by Direct Blending of Epoxidized Soybean Oil, *Fib. Polym*., 21(12), 2949–2961(2020). https://doi.org/10.1007/s12221-020-0111-6

Mostoni, S., Milana, P., Marano, C., Conzatti, L., Mauri, M., D'Arienzo, M., Di Credico, B., Simonutti, R., Stagnaro, P. and Scotti, R., Localizing the cross-links distribution in elastomeric composites by tailoring the morphology of the curing activator, *Compos. Sci. Technol.,* 230, 109780(2022). https://doi.org/10.1016/j.compscitech.2022.109780

Nabil, G. M., Mahmoud, M. E. and Makled, S. O., Green synthesis of novel magnetite mixed metal oxides with cationic surfactant nanocomposite: Investigation of its effective removal of Azorubine E122 food dye and antimicrobial activity, *Appl. Organomet. Chem*., 37(4), e6996(2023). https://doi.org/10.1002/aoc.6996

Nizamlioglu, N. M., Yasar, S. and Bulut, Y., Chemical versus infrared spectroscopic measurements of quality attributes of sun or oven dried fruit leathers from apple, plum and apple-plum mixture, 153, 112420(2022). https://doi.org/10.1016/j.lwt.2021.112420

Raja, T. and Devarajan, Y., Effective utilization of fibre extracted from the waste neem tree twigs—a step towards sustainable practices, *Biomass Convers. Biorefine.,* 14(17), 21049–21057(2024). https://doi.org/10.1007/s13399-023-04133-9

Sathisha, H. C., Krishnamurthy, G. and Nagaraju, G., Facile green synthesis of ZnO/ZrO_2 nanocomposite for photocatalytic degradation and chromium (VI) reduction, *J. Cryst. Growth.,* 651, 128009(2025). https://doi.org/10.1016/j.jcrysgro.2024.128009

Shailaja, N. R., Arulmozhi, M., Balraj, B. and Siva, C., Corallocarpus epigaeus mediated synthesis of ZnO/CuO integrated ZrO_2 nanoparticles for enhanced in-vitro antibacterial, antifungal and antidiabetic activities, *J. Ind. Chem. Soc*., 100(5), 100991(2023). https://doi.org/10.1016/j.jics.2023.100991

Shakil, S. R., Yeasmin, M. N., Asif, S. M. R., Nila, U. H. and Mottalib, M. A., Preparation and Characterization of Ethylene Vinyl Acetate-Based Composites from Footwear Scraps and Peanut Fiber for Value-Added Products, *Fib. Polym*., 26(5), 2159–2174(2025). https://doi.org/10.1007/s12221-025-00943-y

Strohmeier, L., Frommwald, H. and Schlögl, S., Digital light processing 3D printing of modified liquid isoprene rubber using thiol-click chemistry, *RSC Adv.,* 10(40), 23607–23614(2020). https://doi.org/10.1039/d0ra04186f

Tuama, M. J. and Alias, M. F., Synthesis of ZnO: ZrO_2 Nanocomposites Using Green Method for Medical Applications, *Karbala Int. J. Modern Sci*., 10(3), 418–430(2024). https://doi.org/10.33640/2405-609X.3366

Unni, R., Rajasekharan, R., Varghese, R., Dalvi, Y. B., Augustine, R. and Mathew, T. J., Ixora coccinea-Extracted Nanocellulose–ZnO Hybrid: A Biocompatible Antimicrobial Scaffold for Wound Healing, *J. Appl. Polym. Sci*., 142(42), e57641 (2025). https://doi.org/10.1002/app.57641

Unni, R., Reshmy, R., Latha, M. S., Philip, E., Sindhu, R., Binod, P., Pandey, A. and Awasthi, M. K., Enhancement of mechanical and thermal properties of Ixora coccinea L. plant root derived nanocellulose using polyethylene glycol-glutaraldehyde system, *Chemosphere,* 298, 134324(2022). https://doi.org/10.1016/j.chemosphere.2022.134324

Vázquez-Sánchez, A. Y., Corfield, R., Sosa, N., Salvatori, D. and Schebor, C., Physicochemical, functional, and sensory characterization of apple leathers enriched with acáchul (Ardisia compressa Kunth) powder, LWT, 146, 111472(2021). https://doi.org/10.1016/j.lwt.2021.111472

Verma, Y. K., Singh, A. K., Paswan, M. K. and Gurmaita, P. K., Preparation and characterization of bamboo based nanocellulose by ball milling and used as a filler for preparation of nanocomposite, *Polym.,* 308, 127396(2024). https://doi.org/10.1016/j.polymer.2024.127396

Wang, S. Y., Wang, H. G. and Shi, Y., Enhanced gas permeability of HyIIR/CB/OMMT composites constructed from hydroxyl groups and OMMT/CB with strong interactions, 31(3), 711–727(2025). https://doi.org/10.1002/vnl.22202

Wang, X. Y., Li, C. F., Kang, H. L., Li, D. H., Fang, Q. H., Li, L. and Yang, F., A Mechanically Robust and Low Heat Build-up Rubber Formed by Isoprene Rubber Assembled with Eucommia Ulmoides Gum via Hydrogen Bonding, *Chinese J. Polym. Sci.,* 44(3), 845-856(2026). https://doi.org/10.1007/s10118-025-3507-3

Wen, J., Bean, R. H., Nayyar, G., Feller, K., Scott, P. J., Williams, C. B. and Long, T. E., Vat Photopolymerization of Synthetic Isoprene Rubber Latexes, *ACS Appl. Polym. Mater.,* 6(4), 2169–2176(2024). https://doi.org/10.1021/acsapm.3c02604

Yu, R., Prabhakar, M. N., Lee, D. W. and Song, J. L., Extraction and Characterization of Nano-cellulose from Local Waste Paper Egg Trays, 19(14), 8582–8592(2022). https://doi.org/10.1080/15440478.2021.1964143